Published OnlineFirst May 14, 2015; DOI: 10.1158/0008-5472.CAN-14-3477

Cancer Research

Noninvasive Imaging of Tumor PD-L1 Expression Using Radiolabeled Anti–PD-L1 Antibodies

Sandra Heskamp[1], Willemijn Hobo[2], Janneke D.M. Molkenboer-Kuenen[1], Daniel Olive[3], Wim J.G. Oyen[1], Harry Dolstra[2], and Otto C. Boerman[1]

Abstract

Antibodies that block the interaction between programmed death ligand 1 (PD-L1) and PD-1 have shown impressive antitumor activity. Patients with tumors expressing PD-L1 are most likely to respond to this treatment. The aim of our study was to develop a noninvasive imaging technique to determine tumor PD-L1 expression *in vivo*. This could allow selection of patients that are most likely to benefit from anti–PD-1/PD-L1 treatment and to monitor PD-L1 expression during therapy. The monoclonal antibody PD-L1.3.1 was radiolabeled with Indium-111 (^{111}In) and characterized using PD-L1–expressing MDA-MB-231 cells. Subsequently, the optimal antibody dose and time point for imaging was determined in mice with MDA-MB-231 xenografts. Finally, SPECT/CT imaging was performed in xenograft models with different PD-L1 expression levels and tumor sections were analyzed for PD-L1 expression using IHC. The optimal antibody dose of ^{111}In-PD-L1.3.1 (K_d = 1 nmol/L) for SPECT/CT imaging was $\leq$1 μg. Highest tumor-to-normal tissue contrast was obtained at days 3 and 7 after injection. ^{111}In-PD-L1.3.1 SPECT/CT showed efficient accumulation in high PD-L1–expressing tumors (MDA-MB-231 and SK-Br-3), whereas no specific uptake was observed in tumors with low or no detectable levels of PD-L1 (SUM149, BT474, and MCF-7). SPECT/CT and autoradiography showed a very heterogeneous distribution of ^{111}In-PD-L1.3.1 within the tumor. In conclusion, this is the first study showing the feasibility of noninvasive *in vivo* imaging of PD-L1 expression in tumors. ^{111}In-PD-L1.3.1 showed efficient and specific uptake in PD-L1 expressing xenografts. This technique may enable patient selection for PD-1 and PD-L1–targeted therapy. *Cancer Res; 75(14); 1–9. ©2015 AACR.*

Introduction

T cells play an essential role in the anticancer immune response. T-cell activation depends on the initial antigen-specific signal, presented via the antigen-loaded MHC to the T-cell receptor, and on activation of the costimulatory molecule CD28 by binding of CD80/86. T cells also express coinhibitory molecules that are capable of downregulating the immune response (1). One major coinhibitory receptor is programmed death 1 (PD-1). PD-1 has two ligands, programmed death ligand-1 (PD-L1) and PD-L2, of which PD-L1 is most widely expressed. Binding of PD-L1 to PD-1 transduces an inhibitory signal to the T cell, resulting in inhibition of T-cell proliferation, reduced secretion of effector cytokines, and potentially exhaustion. By upregulating PD-L1 expression levels, tumor cells are capable of escaping immune recognition and attack (2–4).

PD-L1 is expressed on a wide variety of tumors, including breast cancer, gastric cancer, renal cell cancer, ovarian cancer, non–small lung cancer, melanoma, and hematologic cancers (5). In general, PD-1 and PD-L1 have been demonstrated to be poor prognostic factors as high-expression levels are associated with poor outcome of cancer patients (5). Preclinical studies with anti–PD-1 and anti–PD-L1 antibodies have shown promising antitumor effects and have led to the initiation of several clinical investigations. Early clinical trials demonstrated objective and durable ($\geq$1 year) responses in patients with treatment-refractory, advanced melanoma, renal cell carcinoma, non–small cell lung cancer, and ovarian cancer (6–11). Because of these impressive results, phase II/III studies are currently further exploring the therapeutic efficacy of these agents. Because of the impressive efficacy in melanoma patients, the FDA has recently granted accelerated approval of pembrolizumab (anti–PD-1 antibody) for the treatment of patients with advanced or unresectable melanoma following progression on prior therapies (11).

Although studies with PD-1/PD-L1–targeted therapies show encouraging results, not all patients respond to this type of treatment and there is an urgent need for a predictive biomarker. In this regard, several studies have postulated that tumor PD-L1 expression might be required for response to anti–PD-1– and anti–PD-L1–targeted therapy (7, 12–14). However, immunohistochemical analysis of PD-L1 expression as determined on archival tissue samples should be interpreted with caution, because PD-L1 expression may undergo changes due to alterations in tumor microenvironment or previous treatment. For example, IFNγ and TNFα can upregulate PD-L1 expression whereas vascular endothelial growth factor (VEGF) can downregulate tumor PD-L1 expression (15–17). Also, certain

[1]Departments of Radiology and Nuclear Medicine, Radboud University Medical Center, Nijmegen, the Netherlands. [2]Laboratory Medicine—Laboratory of Hematology, Radboud University Medical Center, Nijmegen, the Netherlands. [3]CRCM, Immunity and Cancer, Inserm, U1068; Institut Paoli-Calmettes; Aix-Marseille Université, UM 105; CNRS, UMR7258, Marseille, France.

Corresponding Author: Sandra Heskamp, Radboud University Medical Center, P.O. Box 9101, 6500 HB Nijmegen, the Netherlands. Phone: 31-24-36-19097; Fax: 31-24-36-18942; E-mail: sandra.heskamp@radboudumc.nl

doi: 10.1158/0008-5472.CAN-14-3477

Published OnlineFirst May 14, 2015; DOI: 10.1158/0008-5472.CAN-14-3477

chemotherapeutics such as doxorubicin can decrease the expression of PD-L1 on the tumor cell surface, whereas radiotherapy and paclitaxel are capable of upregulating PD-L1 expression (18–20). There are no strict criteria to define PD-L1 positivity by IHC (e.g., cytoplasmic vs. membranous staining, number of positive tumor cells), and misinterpretation may occur due to heterogeneous expression within or between tumor lesions (e.g., primary vs. metastatic lesions; refs. 7, 12–14).

Molecular *in vivo* imaging with radiolabeled anti–PD-L1 antibodies may overcome some of the limitations of immunohistochemical analysis of PD-L1 expression in tumor biopsies. It allows measurement of PD-L1 expression at time of start of therapy, of whole tumor lesions and their metastases, thereby avoiding sampling errors and, thus, misinterpretation due to intratumoral and interlesional heterogeneity. This may result in more accurate detection of PD-L1 expression and accessibility, compared with immunohistochemical analysis. It can potentially be used as biomarker to select patients for PD-1/PD-L1–targeted therapy, and it allows longitudinal monitoring of PD-L1 expression during disease progression and treatment.

Therefore, the aim of this study was to develop a noninvasive *in vivo* imaging technique to measure tumor PD-L1 expression and accessibility. For this purpose, the anti–PD-L1 antibody PD-L1.3.1 was radiolabeled with Indium-111 (^{111}In) and tumor targeting was analyzed by SPECT/CT imaging in mice bearing subcutaneous cancer xenografts with different PD-L1 expression levels.

Materials and Methods

Cell culture

The breast cancer cell lines MDA-MB-231, SK-Br-3, and MCF-7 were cultured in RPMI-1640 (GIBCO, BRL Life Sciences Technologies), supplemented with 2 mmol/L glutamine (GIBCO) and 10% FCS (Sigma-Aldrich Chemie BV) at 37°C in a humidified atmosphere with 5% CO_2. SUM149 was cultured in Ham's F12 medium (GIBCO) supplemented with 5% FCS, 10 mmol/L 4-(2-hydroxyethyl)-1-piperazineethanesulfonic acid (HEPES, GIBCO), hydrocortisone (1 μg/mL, Sigma-Aldrich Chemie BV), and insulin (5 μg/mL, Sigma-Aldrich Chemie BV). BT474 was cultured in RPMI-1640, 2 mmol/L glutamine, 10% FCS, and 10 μg/mL insulin.

FACS analysis of PD-L1 expression

PD-L1 expression of MDA-MB-231, SK-Br-3, SUM149, BT474, and MCF-7 cells was determined by FACS analysis. Cells were incubated with PD-L1-PE (557924; BD Biosciences) or mouse IgG1-PE (400114; Biolegend) for 30 minutes at 4°C. Cells were washed and, subsequently, analyzed using the Gallios flow cytometer (Beckman Coulter).

Radiolabeling

The murine monoclonal IgG1 antibody PD-L1.3.1 is specifically directed against human PD-L1 and does not cross react with murine PD-L1 (21). It was conjugated with isothiocyanatobenzyl-diethylenetriaminepentaacetic acid (ITC-DTPA, Macrocyclis) in 0.1 mol/L $NaHCO_3$, pH 9.5, at a 21-fold molar excess of ITC-DTPA, for 1 hour at room temperature (RT). Unbound ITC-DTPA was removed from the reaction mixture by dialysis against 0.1 mol/L 2-(N-morpholino)ethanesulfonic acid (MES; Sigma-Aldrich Chemie BV) buffer, followed by purification on a disposable G25M Sephadex column (PD10, GE Healthcare Life Sciences, Eindhoven), eluted with 0.25 mol/L ammoniumacetate buffer, pH 5.4 (Sigma-Aldrich Chemie BV).

DTPA-conjugated PD-L1.3.1 was incubated with ^{111}In (Mallinckrodt BV) in 0.5 mol/L MES buffer, pH 5.4, 20 minutes at RT, under strict metal-free conditions (22). After incubation, 50 mmol/L ethylenediaminetetraacetic acid (EDTA) was added to a final concentration of 5 mmol/L to chelate unincorporated ^{111}In. Labeling efficiency was determined using instant thin-layer chromatography on silica gel chromatography strips (Agilent Technologies), using 0.1 mol/L citrate buffer (Sigma-Aldrich Chemie BV), pH 6.0, as the mobile phase. In case labeling efficiency was below 95%, the reaction mixture was purified on a PD-10 column, eluted with PBS, containing 0.5% BSA (Sigma-Aldrich Chemie BV). Radiochemical purity of ^{111}In-DTPA-PD-L1.3.1 (^{111}In-PD-L1.3.1) exceeded 95% in all experiments.

In vitro assays

Binding to breast cancer cell lines. The breast cancer cell lines MDA-MB-231, SK-Br-3, SUM149, BT474, and MCF-7 were cultured to confluency in 6-well plates and incubated with 32 pmol/L ^{111}In-PD-L1.3.1 (1 kBq) for 4 hours at 37°C in a humidified atmosphere with 5% CO_2, or for 4 hours on ice, in RPMI-1640 containing 0.5% BSA. Separate wells were coincubated with a 1,000-fold excess of unlabeled PD-L1.3.1 to determine nonspecific binding. After incubation, cells were washed with PBS and the cell-associated activity was measured in a shielded well-type gamma counter (Perkin-Elmer). Specific binding was calculated by subtracting the nonspecific binding from the total binding.

Immunoreactive fraction. The immunoreactive fraction of ^{111}In-PD-L1.3.1 was determined essentially as described by Lindmo and colleagues (26). A serial dilution of MDA-MB-231 cells (3.3×10^5–8.4×10^7 cells/mL) in RPMI-1640 containing 0.5% BSA was incubated with 8 pmol/L ^{111}In-PD-L1.3.1 (0.2 kBq). Nonspecific binding was determined by adding an excess of unlabeled PD-L1.3.1 (67 nmol/L) to a duplicate of the lowest cell concentration. After 1-hour incubation at 37°C, cells were centrifuged and the activity in the cell pellet was measured in a shielded 3-inch well-type gamma counter (Perkin-Elmer). The inverse of the specific cell bound activity was plotted against the inverse of the cell concentration, and the immunoreactive fraction was calculated from the *y*-axis intercept using GraphPad Prism (version 5.03 for Windows).

IC_{50}. MDA-MB-231 cells were cultured to confluency in 6-well plates. The 50% IC_{50} of PD-L1.3.1 blocking of ^{111}In-PD-L1.3.1 binding was determined by incubating the cells for 4 hours on ice in 1 mL RPMI-1640 0.5% BSA, containing 20 pmol/L ^{111}In-PD-L1.3.1 (1 kBq) and increasing concentrations of unlabeled PD-L1.3.1 (1–1,000 pmol/L). After incubation, cells were washed with PBS and the cell-associated activity was measured in a gamma counter. The IC_{50} was defined as the antibody concentration that was required to inhibit binding of the radiolabeled antibody by 50%. IC_{50} values were calculated using GraphPad Prism.

Scatchard analysis. Scatchard analysis was performed to determine the dissociation constant (K_d) of ^{111}In-PD-L1.3.1 and to

Published OnlineFirst May 14, 2015; DOI: 10.1158/0008-5472.CAN-14-3477

quantitatively measure PD-L1 expression on MDA-MB-231, SK-Br-3, and SUM149 cells. Cells were cultured to confluency in 6-well plates and were incubated for 4 hours on ice with increasing concentrations ^{111}In-PD-L1.3.1 (3–3,000 pmol/L) in 1 mL RPMI-1640 containing 0.5% BSA. Nonspecific binding was determined by coincubation with 100 nmol/L PD-L1.3.1. After incubation, cells were washed with PBS and the cell-associated activity was measured in a shielded well-type gamma counter. The specific binding (total binding—nonspecific binding) was plotted against the bound/free ratio. Data were analyzed by linear regression to determine PD-L1 receptor density per cell and to determine the K_d of ^{111}In-PD-L1.3.1.

Internalization kinetics. MDA-MB-231 cells were cultured in 6-well plates and were incubated for 2, 4, or 24 hours with 75 pmol/L ^{111}In-PD-L1.3.1 (1 kBq) in RPMI-1640 containing 0.5% BSA at 37°C in a humidified atmosphere with 5% CO_2. Nonspecific binding and internalization was determined by coincubation with 17 nmol/L unlabeled PD-L1.3.1. After incubation, acid wash buffer (0.1 mol/L HAc, 0.15 mol/L NaCl, pH 2.6) was added for 10 minutes to remove the membrane-bound fraction of the cell-associated ^{111}In-PD-L1.3.1. Subsequently, cells were harvested from the 6-well plates and the amount of membrane bound and internalized activity was measured in a gamma counter. Specific binding and internalization were calculated by subtracting the nonspecific binding and internalization from the total binding and internalization.

Animal studies

Animal experiments were performed on female BALB/c nude mice (Janvier) and were conducted in accordance with the principles laid out by the revised Dutch Act on Animal Experimentation (1997) and approved by the institutional Animal Welfare Committee of the Radboud University Nijmegen. At 6 to 8 weeks of age, mice were inoculated s.c. with 5×10^6 MDA-MB-231, SK-Br-3, SUM149, MCF-7, or BT474 cells (mixed 2:1 with Matrigel, BD Biosciences; Pharmingen). Mice receiving MCF-7 or BT474 cells were, before tumor cell inoculation, implanted s.c. with a slow release estradiol pellet (0.18 mg, 60 days, Innovative Research of America) under general anesthesia (isoflurane/O_2). Experiments started when tumors reached a size of approximately 0.1 cm^3.

Dose optimization. Seven groups ($n = 6$) of mice with subcutaneous MDA-MB-231 xenografts received an intravenous injection of 0.2 MBq ^{111}In-PD-L1.3.1 (specific activity 0.4 MBq/μg) in the tail vein. To study the effect of the antibody protein dose on the biodistribution of ^{111}In-PD-L1.3.1, groups received increasing protein doses of PD-L1.3.1 (0.3–300 μg/mouse). Three days after injection, mice were euthanized using CO_2/O_2-asphyxiation. The biodistribution of the radiolabel was determined *ex vivo*. Tumor, blood, muscle, lung, heart, spleen, pancreas, intestine, kidney, liver, bone, and bone marrow were dissected and weighed. Activity was measured in a gamma counter. To determine the uptake of radiolabeled antibodies in each sample as a fraction of the injected dose, aliquots of the injected dose were counted simultaneously. The results were expressed as percentage injected dose per gram tissue (%ID/g).

Biodistribution studies. Three groups ($n = 6$) of mice with subcutaneous MDA-MB-231 xenografts and three groups with MCF-7 xenografts received an i.v. injection of 0.2 MBq ^{111}In-PD-L1.3.1. Separate groups of mice were coinjected with an excess of 300 μg unlabeled PD-L1.3.1 to block PD-L1 *in vivo*. At 1, 3, and 7 days after injection of radiolabeled PD-L1.3.1, mice were euthanized, and the *ex vivo* biodistribution of radiolabeled PD-L1.3.1 was determined as described previously.

SPECT/CT imaging. Three mice with subcutaneous MDA-MB-231 and 3 mice with subcutaneous MCF-7 xenografts received an i.v. injection of 15.5 MBq ^{111}In-PD-L1.3.1 (protein dose 1.5 μg). Immediately after injection and 1, 3, and 7 days after injection, images were acquired with the U-SPECT-II/CT (MILabs; ref. 23). Mice were scanned under general anesthesia (isoflurane/O_2) for 30 to 90 minutes using the 1.0-mm diameter pinhole mouse high sensitivity collimator tube, followed by a CT scan (spatial resolution 160 μm, 65 kV, 615 μA) for anatomical reference. Scans were reconstructed with MILabs reconstruction software, using an ordered-subset expectation maximization algorithm, with a voxel size of 0.2 mm. SPECT/CT scans were analyzed and maximum intensity projections (MIP) were created using the Inveon Research Workplace software (IRW, version 4.1). A 3D volume of interest was drawn around the tumor and uptake was quantified as the percentage injected dose per gram (%ID/g), assuming a tissue density of 1 g/cm^3.

^{111}In-PD-L1 SPECT/CT in breast cancer models with different PD-L1 expression levels. Tumor targeting of ^{111}In-PD-L1.3.1 to MDA-MB-231, SK-Br-3, SUM149, MCF-7, and BT474 xenografts was determined in 10 mice bearing subcutaneous tumors on both flanks ($n = 2$ mice/4 tumors/xenograft model). Mice received intravenous tail vein injections of 1 μg (10 MBq) ^{111}In-PD-L1.3.1 and 3 days later, mice were euthanized by CO_2/O_2 asphyxation and SPECT/CT images were acquired for 90 minutes, as described previously. Subsequently, the *ex vivo* biodistribution of radiolabeled PD-L1.3.1 was determined. Tumors were fixed in 4% formalin or frozen at −80°C for autoradiography and IHC.

Autoradiography

Frozen and formalin-fixed tumor sections (5 μm) from mice injected with 10 MBq of ^{111}In-PD-L1.3.1 (1 μg) were exposed to a Fujifilm BAS cassette 2025 overnight (Fuji Photo Film). Phospholuminescence plates were scanned using a Fuji BAS-1800 II bioimaging analyzer at a pixel size of 50 × 50 μm. Images were analyzed with Aida Image Analyzer software (Raytest).

Immunohistochemistry

Frozen tumor sections of MDA-MB-231, SK-Br-3, SUM149, BT474, and MCF-7 were fixed for 10 minutes in ice-cold acetone (−20°C). Endogenous mouse Ig staining was blocked using a mouse-on-mouse blocking kit (BMK-2202, Vector). Subsequently, sections were incubated with 10 μg/mL PD-L.3.1, followed by incubation with a peroxidase-conjugated rabbit-anti-mouse antibody (P0260, DAKO). Finally, 3-3′-Diaminobenzidine (DAB) was used to visualize peroxidase activity in the sections.

Statistical analyses

Statistical analyses were performed using PASW Statistics version 18.0 and GraphPad Prism version 5.03 for Windows.

Published OnlineFirst May 14, 2015; DOI: 10.1158/0008-5472.CAN-14-3477

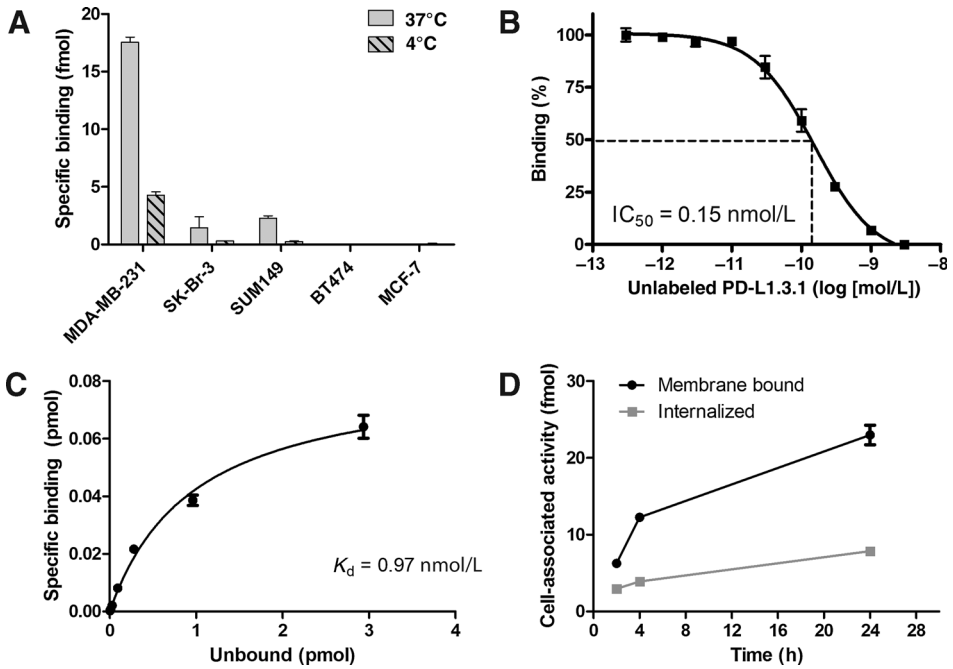

Figure 1.
A, binding of ^{111}In-PD-L1.3.1 to five different breast cancer cell lines. B, IC_{50} analysis of PD-L1.3.1. C, scatchard analysis of ^{111}In-PD-L1.3.1. D, internalization kinetics of ^{111}In-PD-L1.3.1.

Differences in uptake of radiolabeled PD-L1.3.1 were tested for significance using the nonparametric Kruskal–Wallis and Mann–Whitney *U* test. The correlation between tumor uptake measured by SPECT and *ex vivo* biodistribution was calculated with the Spearman correlation coefficient. A *P* value below 0.05 was considered significant.

Results

^{111}In-PD-L1.3.1 specifically binds to PD-L1

Flow-cytometry analysis showed that the percentage of tumor cells positive for PD-L1 was 89.4%, 2.9%, 8.9%, 0.2%, and 0.1% for MDA-MB-231, SK-Br-3, SUM149, BT474, and MCF-7, respectively. PD-L1.3.1 was labeled with ^{111}In, obtaining specific activities up to 10 MBq/μg antibody. ^{111}In-PD-L1.3.1 showed the highest binding to MDA-MB-231 cells while binding to SUM149 and SK-Br-3 was significantly lower ($P = 0.002$). PD-L1–negative BT474 and MCF-7 cells did not show any specific binding of ^{111}In-PD-L1.3.1 (Fig. 1A). The number of binding sites for PD-L1.3.1 was determined quantitatively with scatchard analysis and was 47,700 ± 2,900 for MDA-MB-231, 2,000 ± 100 for SK-Br-3, and 3,600 ± 400 for SUM149. On the basis of these results, MDA-MB-231 cells were used in subsequent binding assays.

The immunoreactive fraction of ^{111}In-PD-L1.3.1 was 82% and the IC_{50} of unlabeled PD-L1.3.1 was 0.15 nmol/L (Fig. 1B). Scatchard analysis showed that the affinity of ^{111}In-labeled PD-L1.3.1 was 0.97 ± 0.15 nmol/L (Fig. 1C). PD-L1.3.1 was slowly internalized by MDA-MB-231 cells. After 24 hours of incubation, 25% of the cell-associated activity was internalized and 75% was still membrane-bound (Fig. 1D). These data demonstrate that ^{111}In-PD-L1.3.1 antibody specifically binds to PD-L1–expressing tumor cells.

^{111}In-PD-L1.3.1 accumulates specifically in PD-L1–positive xenografts

The antibody protein dose-escalation study showed high and specific tumor accumulation of ^{111}In-PD-L1.3 (Fig. 2A). Tumor uptake in PD-L1–positive MDA-MB-231 was the highest in mice injected with 0.3 or 1 μg of antibody (37.5 ± 12.5 and 35.7 ± 5.8%ID/g, respectively, Fig. 2A). At antibody doses of ≥3 μg, tumor uptake significantly decreased (3 μg: 16.9 ± 3.8%ID/g, $P = 0.002$). Tumor uptake was the lowest in mice injected with 300 μg PD-L1.3.1 (7.6 ± 1.6%ID/g). Other organs did not show specific targeting of ^{111}In-PD-L1.3.1.

Uptake of ^{111}In-PD-L1.3.1 by PD-L1–positive MDA-MB-231 xenografts was observed as early as 1 day after injection and further increased at days 3 and 7 (Table 1, Fig. 2B). PD-L1–negative MCF-7 xenografts did not show specific uptake at any time point. Tumor-to-blood ratios increased over time for MDA-MB-231 and were the highest 7 days post injection (3.9 ± 1.0). Tumor-to-blood ratios for MCF-7 did not exceed 0.9 and were not significantly increased compared with the tumor–blood ratios in mice that received an excess of unlabeled PD-L1.3.1. These data demonstrate that ^{111}In-PD-L1.3.1 can discriminate between PD-L1–positive and PD-L1–negative xenografts.

SPECT/CT visualizes PD-L1–positive xenografts

MDA-MB-231 xenografts were clearly visualized with ^{111}In-PD-L1.3.1 SPECT/CT, with increasing contrast between the tumor and normal tissue with time. Typical examples of SPECT/CT scans, and the quantification of tumor and liver uptake are presented in Fig. 3. Tumor uptake in MDA-MB-231 xenografts increased over time, whereas the uptake in MCF-7 xenografts did not exceed uptake in normal organs, such as the liver. Intratumoral distribution of ^{111}In-PD-L1.3.1 was heterogeneous, as is visualized in a zoomed high-resolution image of the tumor in Fig. 3B. There was a strong correlation between the tumor uptake as measured by SPECT and by counting of dissected tissues at 7 days postinjection (Spearman $r = 0.94$).

^{111}In-PD-L1 SPECT/CT can discriminate xenografts with high and low PD-L1 expression levels

SPECT/CT images demonstrated high uptake of ^{111}In-PD-L1.3.1 in MDA-MB-231 and SK-Br-3 xenografts and low uptake

Published OnlineFirst May 14, 2015; DOI: 10.1158/0008-5472.CAN-14-3477

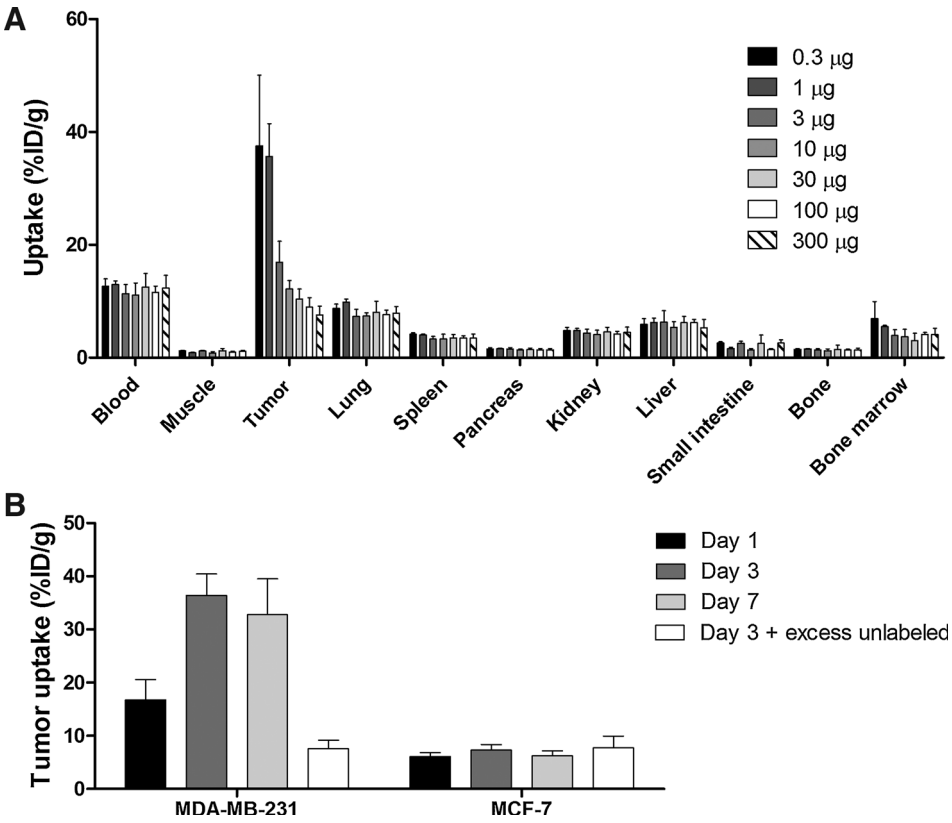

Figure 2.
A, dose-escalation study of ^{111}In-PD-L1.3.1 in mice with subcutaneous MDA-MB-231 xenografts 3 days after injection. B, tumor uptake of ^{111}In-PD-L1.3.1 (1 μg) in mice with subcutaneous MDA-MB-231 or MCF-7 xenografts. Separate groups of mice were injected with an excess of unlabeled PD-L1.3.1.

in SUM149, BT474, and MCF-7 xenografts (Fig. 4), which was confirmed in the *ex vivo* biodistribution study. Tumor uptake at 3 days after injection was 25.2 ± 2.9%ID/g, 22.0 ± 5.1%ID/g, 8.4 ± 0.2%ID/g, 10.0 ± 0.7%ID/g, and 8.1 ± 1.4%ID/g, for MDA-MB-231, SK-Br-3, SUM149, BT474, and MCF-7 xenografts, respectively.

Autoradiographic analysis of the tumor sections showed that ^{111}In-PD-L1.3.1 antibody was distributed heterogeneously within the tumor. In general, highest tumor uptake was observed in the periphery of the tumor, whereas the uptake in the tumor center was lower. This heterogeneous distribution was also observed on cross-sections of the SPECT/CT scan (Fig. 5). After autoradiographic analysis, the same slides were used for hematoxylin and eosin (H&E) staining, which showed that the tumors contained areas with vital tissue (mostly in the periphery of the tumor) and areas with necrosis (mostly in the center of the tumor). In MDA-MB-231 and SK-Br-3 xenografts, highest uptake of ^{111}In-PD-L1.3.1 was found in the vital part of the tumor.

Immunohistochemical analysis of tumor sections for PD-L1 expression showed that MDA-MB-231 tumors expressed the highest levels of PD-L1. SK-Br-3 xenografts also clearly expressed PD-L1, although the expression levels varied largely between the tumors. Immunostaining of SUM149, BT474, and MCF-7 showed low PD-L1 expression (Fig. 5).

In summary, ^{111}In-PD-L1.3.1 SPECT/CT can discriminate between xenografts with high and low PD-L1 expression levels.

Table 1. Tumor targeting of ^{111}In-PD-L1.3.1 to MDA-MB-231 and MCF-7 xenografts at 1, 3, and 7 days after injection

Xenograft	Tumor uptake (%ID/g)	Tumor-to-blood ratio
MDA-MB-231		
Day 1	16.8 ± 3.8	1.1 ± 0.2
Day 3	36.4 ± 4.0	3.1 ± 0.2
Day 7	32.8 ± 6.8	3.9 ± 1.0
Day 3 + excess unlabeled	7.6 ± 1.6	0.6 ± 0.1
MCF-7		
Day 1	6.1 ± 0.7	0.5 ± 0.1
Day 3	7.3 ± 1.0	0.8 ± 0.1
Day 7	6.2 ± 1.0	0.9 ± 0.2
Day 3 + excess unlabeled	7.7 ± 2.2	0.8 ± 0.2

Discussion

Patients with PD-L1–expressing tumors have a poor prognosis. By upregulating PD-L1, tumor cells can escape immune recognition and attack. Anti–PD-1/PD-L1 antibodies have shown impressive antitumor effects. However, currently, there is no useful biomarker to predict response to anti–PD-1/PD-L1 targeted therapy, although there are first indications that tumor PD-L1 expression seems to be required for response to treatment. We have shown for the first time that it is feasible to noninvasively detect tumor PD-L1 expression. SPECT/CT imaging with the monoclonal antibody PD-L1.3.1 showed specific and efficient accumulation in PD-L1–expressing xenografts, whereas no specific uptake was measured in PD-L1–negative tumors.

Molecular imaging with radiolabeled anti–PD-L1 antibodies has important advantages over immunohistochemical analysis

Published OnlineFirst May 14, 2015; DOI: 10.1158/0008-5472.CAN-14-3477

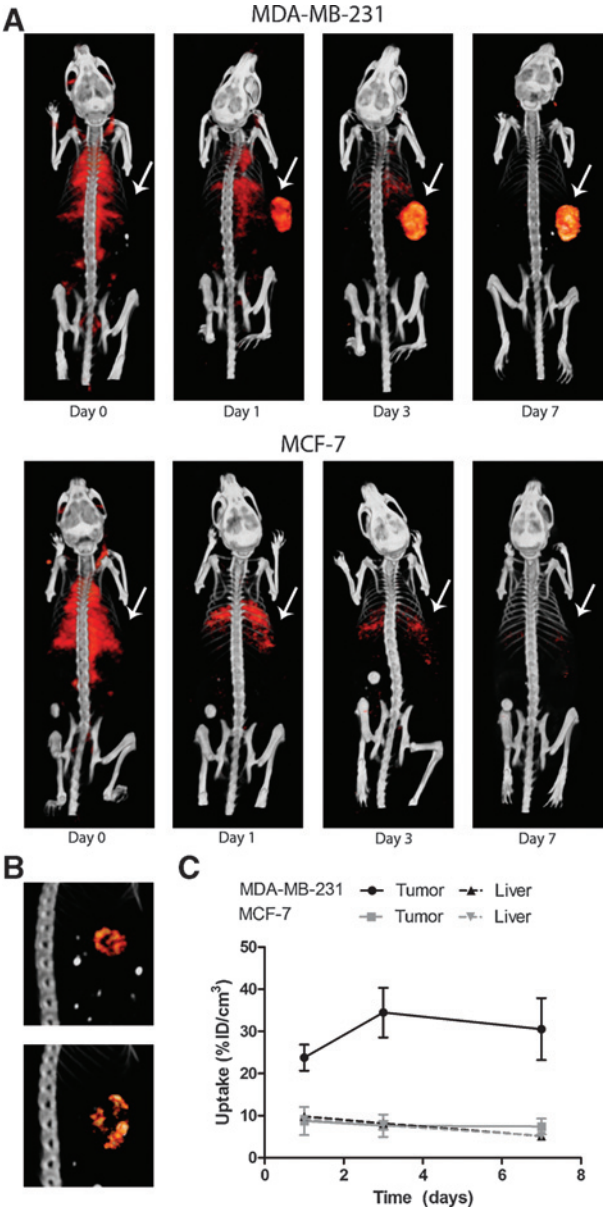

Figure 3.
A, typical examples of SPECT/CT scans of mice with subcutaneous MDA-MB-231 or MCF-7 xenografts, acquired at different time points after injection of 15.5 MBq ^{111}In-PD-L1.3.1 (1.5 μg). Tumors are indicated with the white arrows. B, close-up of the heterogeneous targeting of ^{111}In-PD-L1.3.1 in MDA-MB-231 xenografts. C, uptake of ^{111}In-PD-L1.3.1 in the tumor and liver of mice bearing subcutaneous MDA-MB-231 or MCF-7 xenografts, as quantified from the SPECT scans.

of PD-L1 expression. First of all, imaging allows measurement of PD-L1 expression of whole tumor lesions and their metastases, thereby avoiding sampling errors and thus misinterpretation due to intratumoral and interlesional heterogeneity. Second, it allows monitoring of expression during the course of disease, without the need of repetitive biopsies. This is of clinical importance because PD-L1 expression can change during the course of disease, due to disease progression and/or the effects of treatment (15, 18, 19). Third, *in vivo* imaging techniques also take into account the *in vivo* target accessibility for agents that are administered systemically. Several factors may determine whether antibodies will reach the tumor cells, such as blood vessel density, vascular permeability, and interstitial fluid pressure (24, 25). Therefore, *in vivo* imaging with radiolabeled anti–PD-L1 antibodies may provide more relevant information about PD-L1 expression and accessibility than IHC, it may allow patient selection for PD-1/PD-L1–targeted therapy, and can be used to monitor PD-L1 expression during the course of disease.

Our *in vitro* studies showed that ^{111}In-PD-L1.3.1 has very good characteristics for *in vivo* imaging. Importantly, the immunoreactivity was retained after radiolabeling, and its affinity for PD-L1 was high ($K_d = 1.0$ nmol/L). Moreover, upon binding of PD-L1.3.1 to the tumor cell, PD-L1.3.1 was slowly internalized. This is a favorable characteristic for imaging, because ^{111}In-DTPA is trapped in the tumor cell after internalization and degradation of the antibody (26). This will result in enhanced tumor-to-background contrast in SPECT/CT imaging. *In vivo* studies showed that optimal contrast between tumor and normal tissue was obtained at antibody protein doses of $\leq$1 μg PD-L1.3.1. At higher antibody doses, the PD-L1–binding sites on the tumor cells became saturated, resulting in decreased contrast in SPECT/CT imaging. Because ^{111}In-PD-L1.3.1 is an intact IgG molecule, the clearance from the circulation was relatively slow. Therefore, the optimal time point for imaging was 3 to 7 days after injection.

To investigate the specificity of ^{111}In-PD-L1.3.1 imaging, we compared the uptake of ^{111}In-PD-L1.3.1 in five breast cancer xenografts with different PD-L1 expression levels. *In vitro* analysis showed that MDA-MB-231 expressed high levels of PD-L1, SK-Br-3, and SUM149 showed moderate to low PD-L1 expression levels and BT474 and MCF-7 did not express PD-L1. *In vivo*, MDA-MB-231 xenografts showed high uptake of ^{111}In-PD-L1.3.1, whereas uptake in BT474 and MCF-7 was significantly lower. The low uptake of ^{111}In-PD-L1.3.1 observed in PD-L1–negative tumors was not PD-L1 mediated, because blocking of PD-L1 with an excess of unlabeled PD-L1.3.1 did not further reduce ^{111}In-PD-L1-3.1 uptake. The nonspecific uptake is most likely due to the enhanced permeability and retention effect. Macromolecules larger than 40 kDa selectively leak out from tumor vessels and accumulate in tumor tissue and not in normal tissue. This is caused by the abnormal architecture of tumor vasculature, lack of effective lymphatic drainage, and the production of vascular mediators such as VEGF, which enhance the extravasation and accumulation of macromolecules into tumor tissue (27). The levels of nonspecific uptake observed with PD-L1.3.1 in MCF-7 and MDA-MB-231 xenografs are in the same range as those observed with other antibodies and in other antigen-negative xenograft models (28–30).

The uptake of ^{111}In-PD-L1.3.1 in the two models with moderate to low PD-L1 expression *in vitro* (SK-Br-3 and SUM149) differed significantly from each other *in vivo*. SK-Br-3 xenografts showed high uptake of ^{111}In-PD-L1.3.1, whereas the uptake in SUM149 was comparable with that in the PD-L1–negative models. The low uptake in SUM149 xenografts may be due to the fact that this is an inflammatory breast cancer xenograft. Inflammatory breast cancers are highly vascular tumors that produce large amounts of VEGF (31–33). It has been shown that VEGF expression negatively correlates with PD-L1 expression, which may explain the low PD-L1 expression level of SUM149 *in vivo* (16).

Published OnlineFirst May 14, 2015; DOI: 10.1158/0008-5472.CAN-14-3477

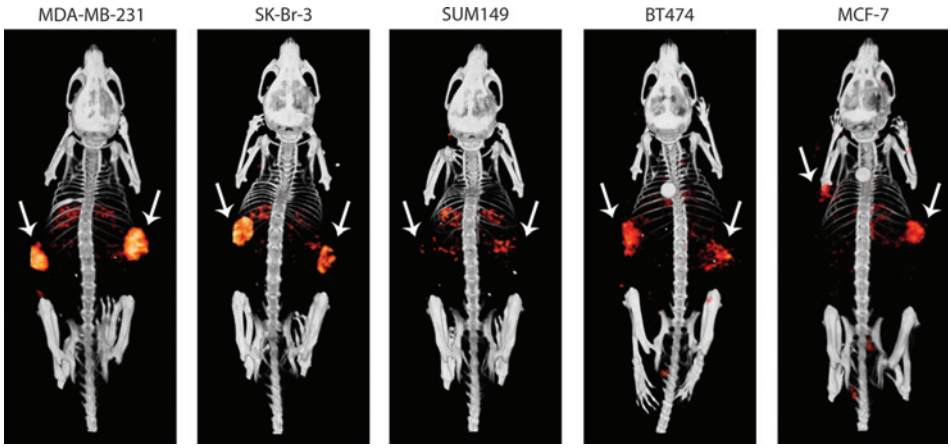

Figure 4.
SPECT/CT scans of mice bearing subcutaneous breast cancer xenografts, with different PD-L1 expression levels, on both flanks (indicated with the white arrows). Scans were acquired 3 days after injection of 10 MBq ^{111}In-PD-L1.3.1 (1 μg). Mean tumor weight was 99 ± 4 mg.

The present preclinical studies show that ^{111}In-PD-L1.3.1 is a promising tracer to noninvasively determine PD-L1 expression and accessibility in cancer lesions. PD-L1.3.1 is specifically directed against human PD-L1, and does not cross react with murine PD-L1. Therefore, in animal models, ^{111}In-PD-L1.3.1 targets PD-L1 expressed on human tumor cells, while it has no affinity for murine PD-L1 expressed on murine cells, such as dendritic cells, macrophages, and natural killer cells (5). In addition, PD-L1 mRNA was found in non-lymphoid tissue such as the heart, skeletal muscles, placenta, and lungs. However, in these tissues, PD-L1 protein expression was not detectable with IHC, indicating that these tissues have very low-expression levels (15, 34, 35). Future *in vivo* studies will have to demonstrate whether tumor targeting of ^{111}In-PD-L1.3.1 is affected by the presence of PD-L1–expressing human cells. Also, to translate noninvasive PD-L1 imaging into the clinic, anti–PD-L1 antibodies should be preferably radiolabeled with the positron emitter zirconium-89 (^{89}Zr) for PET/CT imaging. For preclinical purposes, microSPECT/CT has a similar or even better resolution compared with microPET/CT. However, in the clinical setting, the resolution, sensitivity, and quantification of PET/CT are superior to that of SPECT/CT.

Immunohistochemical analysis of PD-L1 expression seemed to correlate with tumor uptake of ^{111}In-PD-L1.3.1, although there were some discrepancies. MDA-MB-231 and SK-Br xenografts both showed clear PD-L1 expression as determined

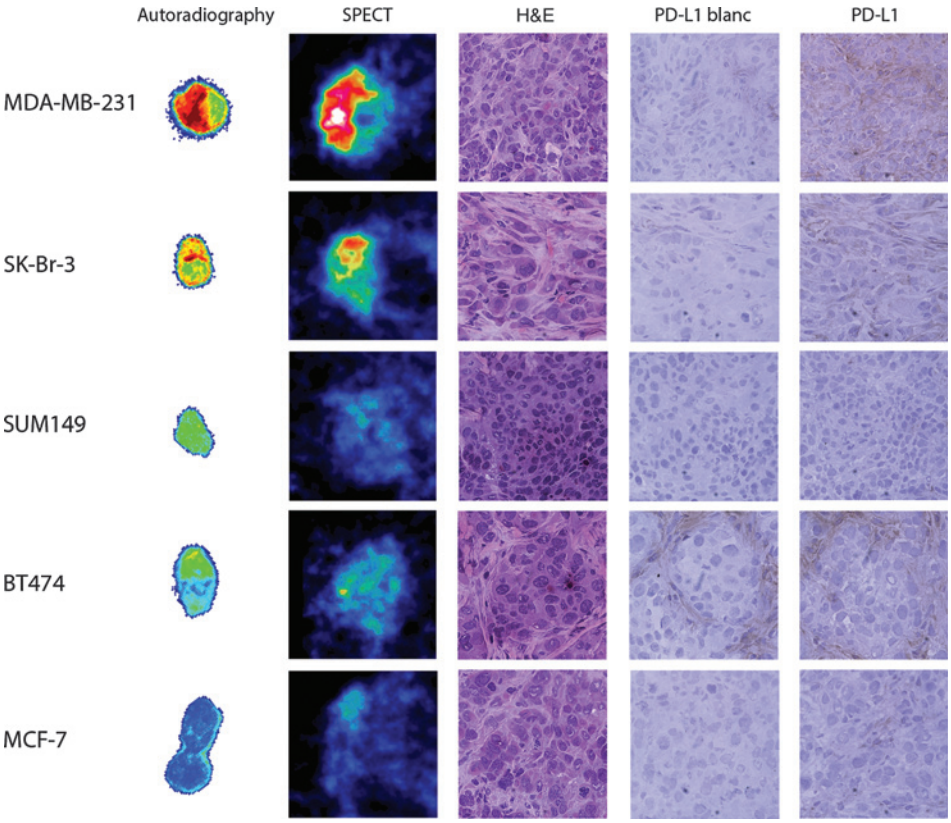

Figure 5.
Examples of autoradiography and cross section of SPECT scans to illustrate the heterogeneous distribution of ^{111}In-PD-L1.3.1 in the xenograft, H&E staining, and PD-L1 immunostaining of breast cancer xenografts.

Published OnlineFirst May 14, 2015; DOI: 10.1158/0008-5472.CAN-14-3477

immunohistochemically and high tumor uptake of ^{111}In-PD-L1.3.1. However, in the PD-L1–negative models (BT474 and MCF-7) that did not show specific uptake of ^{111}In-PD-L1.3.1, we also observed some immunostaining for PD-L1. This illustrates the difficulty to adequately score PD-L1 expression in immunohistochemically stained sections. At the moment, there are no strict criteria to define PD-L1 positivity (e.g., cytoplasmic vs. membranous staining, intensity of the staining, percentage of positive cells) and different immunohistochemical staining procedures have been reported in literature (7, 12–14).

Next to PD-L1 expression, other biomarkers have been studied for their potential to predict response to PD-1/PD-L1–targeted therapy. Several immunohistochemical features, including PD-1, PD-L1, and PD-L2 expression, patterns of immune cell filtration, and lymphocytes subpopulations, have been analyzed for their association with clinical outcome after treatment with anti–PD-1/PD-L1 antibodies. These studies showed that tumor cell PD-L1 expression significantly correlated with objective response, whereas PD-L2 expression did not (12–14, 36). Also, PD-1 expression and the presence of tumor-infiltrating lymphocytes did not correlate to response to anti–PD-1 antibodies (12). Thus, so far, PD-L1 expression seems to be the most powerful predictor of response to both PD-1– and PD-L1–targeted therapy.

Conclusion

This study shows the feasibility to noninvasively determine PD-L1 expression and accessibility of tumor lesions using radiolabeled anti–PD-L1 antibodies and SPECT/CT imaging. These encouraging results warrant future research to explore the feasibility of this approach in patients. Ultimately, this imaging technique may serve as biomarker to predict clinical response to PD-1/PD-L1–targeted therapy.

Disclosure of Potential Conflicts of Interest

No potential conflicts of interest were disclosed.

Authors' Contributions

Conception and design: S. Heskamp, W. Hobo, H. Dolstra, O.C. Boerman
Development of methodology: S. Heskamp, J.D.M. Molkenboer-Kuenen, D. Olive, O.C. Boerman
Acquisition of data (provided animals, acquired and managed patients, provided facilities, etc.): S. Heskamp, W. Hobo, J.D.M. Molkenboer-Kuenen, H. Dolstra
Analysis and interpretation of data (e.g., statistical analysis, biostatistics, computational analysis): S. Heskamp, J.D.M. Molkenboer-Kuenen, W.J.G. Oyen
Writing, review, and/or revision of the manuscript: S. Heskamp, W. Hobo, J.D.M. Molkenboer-Kuenen, W.J.G. Oyen, H. Dolstra, O.C. Boerman
Administrative, technical, or material support (i.e., reporting or organizing data, constructing databases): S. Heskamp, J.D.M. Molkenboer-Kuenen
Study supervision: S. Heskamp, D. Olive, O.C. Boerman

Acknowledgments

The authors thank Bianca Lemmers-van de Weem, Henk Arnts, Iris Lamers-Elemans, and Kitty Lemmens-Hermans for technical assistance with the animal experiments.

The costs of publication of this article were defrayed in part by the payment of page charges. This article must therefore be hereby marked *advertisement* in accordance with 18 U.S.C. Section 1734 solely to indicate this fact.

Received December 3, 2014; revised March 11, 2015; accepted March 30, 2015; published OnlineFirst May 14, 2015.

References

1. Riella LV, Paterson AM, Sharpe AH, Chandraker A. Role of the PD-1 pathway in the immune response. Am J Transplantat 2012;12:2575–87.
2. Hamid O, Carvajal RD. Anti-programmed death-1 and anti-programmed death-ligand 1 antibodies in cancer therapy. Expert Opin Biol Ther 2013;13:847–61.
3. Saresella M, Rainone V, Al-Daghri NM, Clerici M, Trabattoni D. The PD-1/PD-L1 pathway in human pathology. Curr Mol Med 2012;12:259–67.
4. Ostrand-Rosenberg S, Horn LA, Haile ST. The programmed death-1 immune-suppressive pathway: barrier to antitumor immunity. J Immunol 2014;193:3835–41.
5. Zou W, Chen L. Inhibitory B7-family molecules in the tumour microenvironment. Nat Rev Immunol 2008;8:467–77.
6. Brahmer JR, Tykodi SS, Chow LQ, Hwu WJ, Topalian SL, Hwu P, et al. Safety and activity of anti-PD-L1 antibody in patients with advanced cancer. N Engl J Med 2012;366:2455–65.
7. Topalian SL, Hodi FS, Brahmer JR, Gettinger SN, Smith DC, McDermott DF, et al. Safety, activity, and immune correlates of anti-PD-1 antibody in cancer. N Engl J Med 2012;366:2443–54.
8. Lipson EJ, Sharfman WH, Drake CG, Wollner I, Taube JM, Anders RA, et al. Durable cancer regression off-treatment and effective reinduction therapy with an anti-PD-1 antibody. Clin Cancer Res 2013;19:462–8.
9. Hamid O, Robert C, Daud A, Hodi FS, Hwu WJ, Kefford R, et al. Safety and tumor responses with lambrolizumab (anti-PD-1) in melanoma. N Engl J Med 2013;369:134–44.
10. Topalian SL, Sznol M, McDermott DF, Kluger HM, Carvajal RD, Sharfman WH, et al. Survival, durable tumor remission, and long-term safety in patients with advanced melanoma receiving nivolumab. J Clin Oncol 2014;32:1020–30.
11. Robert C, Ribas A, Wolchok JD, Hodi FS, Hamid O, Kefford R, et al. Anti-programmed-death-receptor-1 treatment with pembrolizumab in ipilimumab-refractory advanced melanoma: a randomised dose-comparison cohort of a phase 1 trial. Lancet 2014;384:1109–17.
12. Taube JM, Klein A, Brahmer JR, Xu H, Pan X, Kim JH, et al. Association of PD-1, PD-1 ligands, and other features of the tumor immune microenvironment with response to anti-PD-1 therapy. Clin Cancer Res 2014;20:5064–74.
13. Grosso J, Horak CE, Inzunza D, Cardona DM, Simon JS, Gupta AK, et al. Association of tumor PD-L1 expression and immune biomarkers with clinical activity in patients (pts) with advanced solid tumors treated with nivolumab (anti-PD-1; BMS-936558; ONO-4538). J Clin Oncol 2013;31:177s.
14. Herbst RS, Gordon MS, Fine GD, Sosman JA, Soria JC, Hamid O, et al. A study of MPDL3280A, an engineered PD-L1 antibody in patients with locally advanced or metastatic tumors. J Clin Oncol 2013;31:173s.
15. Dong H, Strome SE, Salomao DR, Tamura H, Hirano F, Flies DB, et al. Tumor-associated B7-H1 promotes T-cell apoptosis: a potential mechanism of immune evasion. Nat Med 2002;8:793–800.
16. Joseph RW, Parasramka M, Eckel-Passow JE, Serie D, Wu K, Jiang L, et al. Inverse association between programmed death ligand 1 and genes in the VEGF pathway in primary clear cell renal cell carcinoma. Cancer Immunol Res 2013;1:378–85.
17. Kondo A, Yamashita T, Tamura H, Zhao W, Tsuji T, Shimizu M, et al. Interferon-gamma and tumor necrosis factor-alpha induce an immunoinhibitory molecule, B7-H1, via nuclear factor-kappaB activation in blasts in myelodysplastic syndromes. Blood 2010;116:1124–31.
18. Ghebeh H, Lehe C, Barhoush E, Al-Romaih K, Tulbah A, Al-Alwan M, et al. Doxorubicin downregulates cell surface B7-H1 expression and upregulates its nuclear expression in breast cancer cells: role of B7-H1 as an anti-apoptotic molecule. Breast Cancer Res 2010;12:R48.
19. Zhang P, Su DM, Liang M, Fu J. Chemopreventive agents induce programmed death-1-ligand 1 (PD-L1) surface expression in breast cancer

Published OnlineFirst May 14, 2015; DOI: 10.1158/0008-5472.CAN-14-3477

cells and promote PD-L1-mediated T cell apoptosis. Mol Immunol 2008; 45:1470–6.
20. Deng L, Liang H, Burnette B, Beckett M, Darga T, Weichselbaum RR, et al. Irradiation and anti-PD-L1 treatment synergistically promote antitumor immunity in mice. J Clin Invest 2014;124:687–95.
21. Ghiotto M, Gauthier L, Serriari N, Pastor S, Truneh A, Nunes JA, et al. PD-L1 and PD-L2 differ in their molecular mechanisms of interaction with PD-1. Int Immunol 2010;22:651–60.
22. Brom M, Joosten L, Oyen WJ, Gotthardt M, Boerman OC. Improved labelling of DTPA- and DOTA-conjugated peptides and antibodies with 111In in HEPES and MES buffer. EJNMMI Res 2012;2:4.
23. van der Have F, Vastenhouw B, Ramakers RM, Branderhorst W, Krah JO, Ji C, et al. U-SPECT-II: an ultra-high-resolution device for molecular small-animal imaging. J Nucl Med 2009;50:599–605.
24. Heldin CH, Rubin K, Pietras K, Ostman A. High interstitial fluid pressure - an obstacle in cancer therapy. Nat Rev Cancer 2004;4:806–13.
25. Jain RK. Transport of molecules, particles, and cells in solid tumors. Annu Rev Biomed Eng 1999;1:241–63.
26. Lindmo T, Boven E, Cuttitta F, Fedorko J, Bunn PA Jr. Determination of the immunoreactive fraction of radiolabeled monoclonal antibodies by linear extrapolation to binding at infinite antigen excess. J Immunol Methods 1984;72:77–89.
27. Fang J, Nakamura H, Maeda H. The EPR effect: unique features of tumor blood vessels for drug delivery, factors involved, and limitations and augmentation of the effect. Adv Drug Deliv Rev 2011;63: 136–51.
28. Dijkers EC, Kosterink JG, Rademaker AP, Perk LR, van Dongen GA, Bart J, et al. Development and characterization of clinical-grade 89Zr-trastuzumab for HER2/neu immunoPET imaging. J Nucl Med 2009;50: 974–81.
29. Heskamp S, van Laarhoven HW, Molkenboer-Kuenen JD, Franssen GM, Versleijen-Jonkers YM, Oyen WJ, et al. ImmunoSPECT and immunoPET of IGF-1R expression with the radiolabeled antibody R1507 in a triple-negative breast cancer model. J Nucl Med 2010;51:1565–72.
30. Marquez BV, Ikotun OF, Zheleznyak A, Wright B, Hari-Raj A, Pierce RA, et al. Evaluation of (89)Zr-pertuzumab in breast cancer xenografts. Mol Pharm 2014;11:3988–95.
31. Heskamp S, Boerman OC, Molkenboer-Kuenen JD, Oyen WJ, van der Graaf WT, van Laarhoven HW. Bevacizumab reduces tumor targeting of anti-epidermal growth factor and anti-insulin-like growth factor 1 receptor antibodies. Int J Cancer 2013;133:307–14.
32. Van der Auwera I, Van Laere SJ, Van den Eynden GG, Benoy I, van Dam P, Colpaert CG, et al. Increased angiogenesis and lymphangiogenesis in inflammatory versus noninflammatory breast cancer by real-time reverse transcriptase-PCR gene expression quantification. Clin Cancer Res 2004; 10:7965–71.
33. Bieche I, Lerebours F, Tozlu S, Espie M, Marty M, Lidereau R. Molecular profiling of inflammatory breast cancer: identification of a poor-prognosis gene expression signature. Clin Cancer Res 2004;10:6789–95.
34. Dong H, Zhu G, Tamada K, Chen L. B7-H1, a third member of the B7 family, co-stimulates T-cell proliferation and interleukin-10 secretion. Nat Med 1999;5:1365–9.
35. Freeman GJ, Long AJ, Iwai Y, Bourque K, Chernova T, Nishimura H, et al. Engagement of the PD-1 immunoinhibitory receptor by a novel B7 family member leads to negative regulation of lymphocyte activation. J Exp Med 2000;192:1027–34.
36. Hodi FS, Powles T, Cassier P, Kowanetz M, Herbst RS, Soria JC, et al. MPDL3280A (anti-PDL1): clinical activity, safety and biomarkers of an engineered PD-L1 antibody in patients with locally advanced or metastatic tumors. Eur J Cancer 2013;49:S184–S.

AACR American Association for Cancer Research

Cancer Research

The Journal of Cancer Research (1916–1930) | The American Journal of Cancer (1931–1940)

Noninvasive Imaging of Tumor PD-L1 Expression Using Radiolabeled Anti–PD-L1 Antibodies

Sandra Heskamp, Willemijn Hobo, Janneke D.M. Molkenboer-Kuenen, et al.

Cancer Res Published OnlineFirst May 14, 2015.